Built-in anionic equilibrium for atom-economic recycling of spent lithium-ion batteries

Pengfei Zhu,[a] Zhipeng Jiang,[a] Wei Sun,[b] Yue Yang,[b] Debbie S. Silvester,[c] Hongshuai Hou,[a] Craig E. Banks,[d] Jiugang Hu*[a] and Xiaobo Ji*[a]

Recycling spent lithium-ion batteries (LIBs) is crucial to address environmental and global sustainability issues. Wet chemical extraction of valuable metals is currently the most practical disposal technology, but it is challenging due to excessive chemical consumption and concomitant secondary pollution. In this study, a built-in anionic equilibrium strategy was proposed to recycle spent $LiFePO_4$ (sLFP) cathodes with high atom economy. The selective extraction of lithium and phosphorus was successfully achieved in deionized water under oxygen pressure by the anionic equilibrium between OH^- produced by oxygen reduction and PO_4^{3-} released from sLFP. The formed $LiFePO_4$·OH phase limited the lithium leaching efficiency to 65.6%, so the trapped lithium was further extracted by rebuilding the anionic equilibrium after adding phosphoric acid with a low H_3PO_4/Li molar ratio. The degraded $LiFePO_4$ evolved into a fusiform $Fe_5(PO_4)_4(OH)_3 \cdot 2H_2O$ crystal, and 90.19% of lithium and 19.88% of phosphorus in sLFP can be recovered as Li_3PO_4 products. This built-in anionic equilibrium mechanism contributes to reduce chemical consumption and high-saline wastewater, thus providing a sustainable hydrometallurgical recycling route for spent lithium-ion batteries.

Introduction

With the rapid development of lithium-ion batteries (LIBs) in electric vehicles and electric storage systems over the last three decades, millions of tons of battery waste will be generated because of their 8–10 year lifespan.[1] For sustainable development of the LIB industry and for environmental protection, recycling of valuable metals from spent/retired LIBs has become a global concern.[2,3] Current recycling technologies for spent LIBs include pyrometallurgy, direct recycling, and wet chemical extraction.[4–6] Although pyrometallurgy is practical for large-scale production owing to its durability for complex chemical compositions, its low recovery efficiency and significant gas emissions are still challenging. Direct recycling retains the original structure and repairs the damaged lattice by replenishing the lithium sources assisted by high-temperature calcination.[7–9] However, obstinate impurities and low consistency of the retired cathode limits its application. In comparison, wet chemical extraction directly recovers the desired elements

[a] College of Chemistry and Chemical Engineering, Central South University, Changsha 410083, China. E-mail: hujiugang@csu.edu.cn, xji@csu.edu.cn; Fax: +86-731-88879616
[b] School of Minerals Processing and Bioengineering, Central South University, Changsha 410083, China
[c] School of Molecular and Life Sciences, Curtin University, GPO Box U1987, Perth, Western Australia 6845, Australia
[d] Faculty of Science and Engineering, Manchester Metropolitan University, Chester Street, Manchester M1 5GD, UK

† Electronic supplementary information (ESI) available. See DOI: https://doi.org/10.1039/d3ee00571b

from spent LIBs with high efficiency, which is widely applicable in the metallurgical industry.[10,11] However, these chemicals are typically wasted and generate significant secondary pollution. Additionally, the large consumption of chemicals reduces the recycling economy, particularly for inexpensive spent $LiFePO_4$ (sLFP) batteries.

Polyanionic lithium iron phosphate cathodes occupy an indispensable market share (B32% in the LIB industry) because of their high thermal stability and long cycle span.[12] Although the values of the main iron and phosphorus components are low, wet chemical recycling of sLFP batteries remains very attractive because of the high grade (1–2%) and value ($70 000 t^{-1}) of the recovered lithium. In the conventional non-selective acid-leaching process, several inorganic acids (H_2SO_4, H_3PO_4 or HNO_3) are used to decompose the sLFP and facilitate effective metal extraction.[13–15] Due to the stable olivine structured $LiFePO_4$, the supplied acid must be greatly excessive to ensure high leaching efficiency of Li and Fe, which increases the recycling cost of sLFP. In addition to expensive chemicals, the excessive acid and introduced inorganic anions are wasted, resulting in large amounts of high-salinity wastewater. Compared with inorganic acid leaching, the combination of oxidants and weak organic acids, such as formic acid,[16,17] acetic acid,[18] or citric acid,[14] achieves selective lithium extraction. Although acid/oxidation synergistic leaching largely reduces acid utilisation, the treatment of the generated organic wastewater may pose a greater challenge. To realise waste-free sLFP recovery, green and sustainable technologies with high atom economy are still being pursued in industry.

Theoretically, the oxidation environment can realise selective delithiation without introducing acid species, similar to the charging process of LFP-based batteries. Several studies have focused on sLFP disposal using individual oxidising agents such as sodium/potassium/ammonium peroxysulphates.[19–21] Although favourable selective leaching of Li with high efficiency was achieved at a low slurry ratio, the atom economy in the entire recovery process is undesirable (less than 60%) considering the reductive SO_4^{2-} species could not be utilised in final Li product. The introducing soluble cations (Na^+ or NH_4^+) also brought complex separation and purification steps. High atom economy and waste-free recycling of sLFP may be achieved if the reductive anions precisely balance the leached Li^+ to form the final Li product such as OH^-, CO_3^{2-}, or PO_4^{3-}, called ''built-in anions''. Hydrogen peroxide can satisfy this requirement considering hydroxide (OH^-) as the sole reductive anion. However, its usage reached 15 vol% at a relatively low solid/liquid ratio (B5 g L^{-1}) owing to the rapid self-decomposition of hydrogen peroxide.[22] Moreover, the upstream synthesis of H_2O_2 is associated with significant economic costs and environmental impact. Compared with the synthetic chemical reagents, oxygen is readily accessible and can be completely reduced as OH^- anion in solution, which is a potential green and sustainable oxidant for sLFP.

In this study, a built-in anionic equilibrium strategy was proposed to directly recover lithium from sLFP batteries in deionized water under oxygen pressure. The built-in equilibrium mechanism is elucidated by detailed element migration and phase identification analyses. Low-stoichiometric phosphoric acid was added to eliminate the leaching bottleneck in the oxygen-rich water system and improved the lithium recovery. The leached lithium and phosphate may be quantitatively recovered as Li_3PO_4 products without producing additional salt-containing wastewater in the entire recycling process. Benefit from the low reagent consumption and high atom economy, this study demonstrates a practical hydrometallurgy recycling route with outstanding efficiency and reduced carbon footprint, thus providing a promising sustainable strategy for large-scale recycling of spent LIB with significant economic and environmental benefits.

Results and discussion

As the principal constituent of air, oxygen is the most common and sustainable oxidizing agent.[23] Theoretically, O_2 can be used to extract Li from sLFP, considering the reducibility of LFP ($LiFePO_4/FePO_4$, 0.380 V *versus* the standard hydrogen electrode (SHE)) and the oxidation potential of O_2 (O_2/OH^-, 0.401 V *versus* SHE). Owing to the low solubility of O_2 in water, the oxygen pressure was modulated in an autoclave to provide a sufficient oxidation atmosphere, as shown in Fig. 1a. After the dissolved O_2 molecules diffused and adsorbed on the surface of the sLFP particles, ferrous iron was oxidised and hydroxyl (OH^-) species were generated according to the typical oxygen reduction reaction. Two built-in anion equilibrium conditions were considered for an oxygen-rich water leaching system. First, the lithium element is selectively extracted from the sLFP lattice, where the olivine structure of LFP remains intact and Fe/P elements remain in the leaching residues in the form of $FePO_4$ (Fig. 1b). The formed OH^- anions can balance the charge of Li^+ in the leachate and form a LiOH solution. Second, the olivine-structured LFP collapses and equimolar Li^+, Fe^{3+}, PO_4^{3-}, and OH^- ions are generated. In an acid-free environment, Fe^{3+} cations readily react with PO_4^{3-} and OH^- anions because of the low k_{sp} values of $Fe(OH)_3$ (2.8×10^{-39})[24] and $FePO_4$ (1.3×10^{-22}).[25] In this case, residual anions (PO_4^{3-} and OH^-) remain in the leachates to balance the leached Li^+, as shown in Fig. 1c.

Based on the measured element concentration in the Table S1 (ESI†), the leaching behaviour of sLFP in oxygen-rich water is depicted in Fig. 1d–f. Under 0.2 MPa of oxygen partial pressure and 2 h of leaching, the leaching efficiency of lithium increased from 25.3% to 57.9% as the temperature increased from 120 to 210 1C, but it clearly declined to 38.1% at 240 1C (Fig. 1d). The leaching behaviour of phosphate species ($H_xPO_4^{-3+x}$, $0 \le x \le 3$, termed as P) with temperature was similar to that of Li; its leaching efficiency increased from 13.1% (120 1C) to 41.6% (210 1C) and then decreased to 28.0% at 240 1C. The significant improvement of both Li and P leaching may be induced by the mediation of oxygen reduction[26,27] and the LFP structure under high temperature.[28] At a leaching temperature of 210 1C, increasing the oxygen partial pressure to a certain amount was favourable for Li leaching. As shown in Fig. 1e, the leaching efficiency of Li increased gradually from 50.5% to 65.6% as the partial oxygen pressure increased from 0.1 to 0.3 MPa. However, further

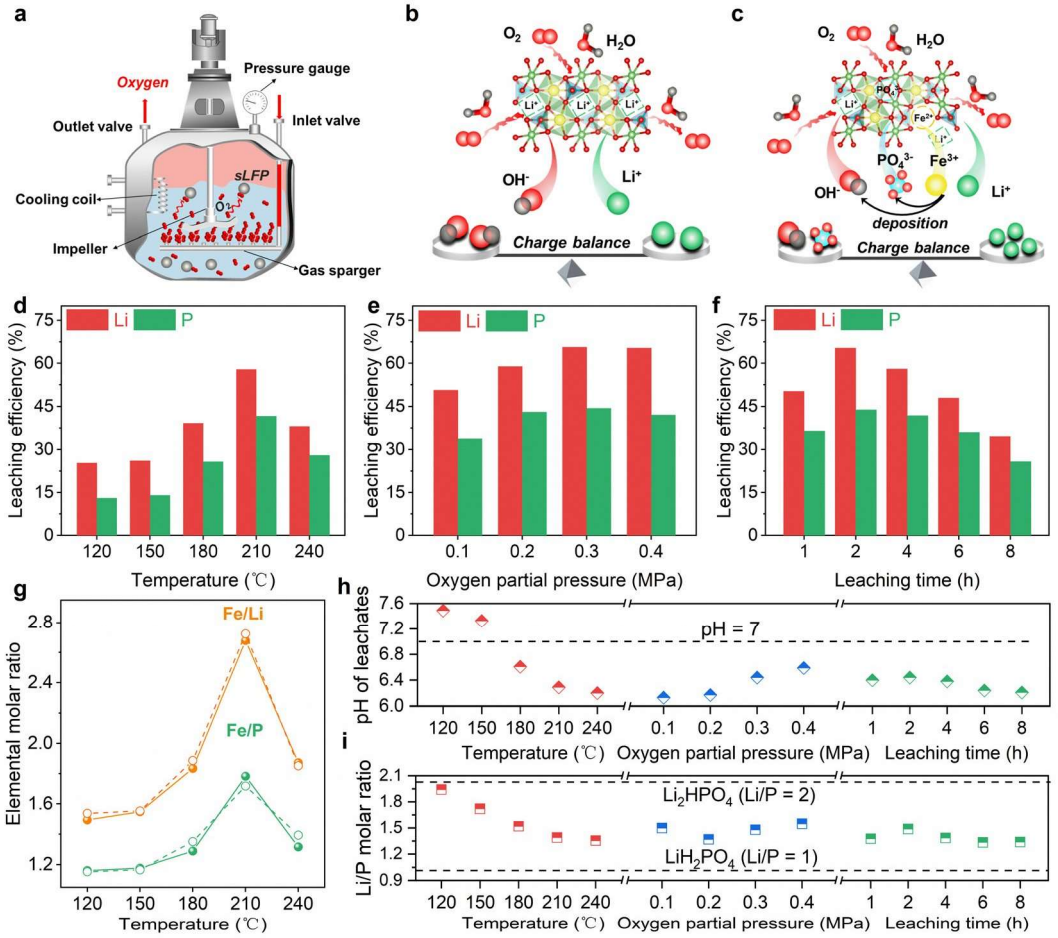

Fig. 1 (a) Schematic of oxygen pressure leaching equipment; (b) hydroxide as the individual anion for equilibrium with leached Li^+; (c) both hydroxide and released phosphate anions for equilibrium with leached Li^+; (d) oxygen-pressure leaching behaviour of sLFP in oxygen-rich water at varied temperature (partial oxygen pressure: 0.2 MPa; leaching time: 2 h), (e) oxygen partial pressure (temperature: 210 ıC, leaching time: 2 h), and (f) leaching time (temperature: 210 ıC, partial oxygen pressure: 0.3 MPa); (g) measured (solid line) and theoretical (dotted line) molar ratios of Fe/Li and Fe/P in the leaching residues at various temperatures; (h) changes in the pH and (i) Li/P molar ratios in the leachates under various experimental conditions, which were determined at 25 ıC.

increasing the oxygen partial pressure to 0.4 MPa did not significantly affect Li leaching. Notably, the leaching efficiency of Li increased from 50.2% at 1 h to 65.3% at 2 h, whereas leached Li and P may return to the residues when the leaching time further extended, which indicates an undesired phase transition (Fig. 1f). Notably, the leaching efficiency of Fe was lower than 0.1% in all leachates (Table S1, ESI†), thus it was not depicted in the Fig. 1d–f. The highest leaching efficiencies for Li and P in the oxygen-rich water were limited to 65.6% and 44.4%, respectively, at 210 ıC and 0.3 MPa of oxygen partial pressure for 2 h.

The detection of P in the leachates indicates that the olivine-structured LFP was destroyed, and the built-in anionic equilibrium mechanism in oxygen-rich water may be identical to that of the second case (Fig. 1c). As shown in Fig. 1g and Fig. S1 (ESI†), the measured molar ratios of Fe/Li and Fe/P in the leaching residues (LRs) were similar to their theoretical values, which were calculated based on the initial elemental composition and the Li/P amounts in the leachates (detailed in the Experimental section). Thus, Fe was remained in the residues throughout the leaching process due to the phase transformation under oxygen pressure. As depicted in the Fig. 1g, the measured Fe/P molar ratio at 210 ıC (1.8) was significantly higher than the initial value in the sLFP (1.0), further demonstrating the leaching of phosphate species in the leachates. However, iron ions were difficult to exist in the circumneutral solution environment (Fig. 1h). The leachates were weakly alkaline (pH 4 7) at temperatures below 180 ıC, which directly confirmed the oxygen reduction behaviour in the oxygen-rich water system. However, the leachates became acidic (pH o 7) as the temperature increased to 210 ıC, which may be due to the formation of the $Li_xH_{3-x}PO_4$ salt. Combining the element leaching behaviours of sLFP, the built-in anionic equilibrium strategy enabled the selective extraction of both Li and P in the oxygen-rich water leaching system. In the circumneutral environment, the amount of OH^- anions in the leachate was negligible; thus, the leached Li^+ was mainly balanced by protonated $H_2PO_4^-$ or HPO_4^{2-} species.

The Li/P molar ratio in the leachates may reflect the formation of $Li_xH_{3-x}PO_4$, which is essential for determining the

recovery process. The released PO_4^{3-} is highly hydrolysed to form LiH_2PO_4 (Li/P = 1), while Fe component can synchronously react with formed OH^-, according to eqn (1). Furthermore, the released PO_4^{3-} undergoes primary hydrolysis to form Li_2HPO_4 (Li/P = 2), while Fe can react with OH^- and PO_4^{3-}, according to eqn (2). As shown in Fig. 1i, the molar ratio of Li/P decreased gradually from 1.94 ($Li_{1.94}H_{1.06}PO_4$) to 1.30 ($Li_{1.30}H_{1.70}PO_4$) as the temperature increased from 120 to 240 ıC, indicating that a mixed reaction process occurred and the built-in anionic equilibrium gradually transformed from eqn (2) to (1). Combined with the change in solution pH and Li/P ratio, it was concluded that temperature is a determining factor for the leaching of sLFP in the oxygen-rich water.

$$4LiFePO_4 + O_2 + 10H_2O - 4LiH_2PO_4 + 4Fe(OH)_3k \quad (1)$$

$$4LiFePO_4 + O_2 + 4H_2O - 2Li_2HPO_4 + 2FePO_4k + 2Fe(OH)_3k \quad (2)$$

Although about two-thirds of lithium was leached in deionized water under oxygen pressure, it still does not satisfy the requirement for sustainable recycling of sLFP. To understand the leaching bottleneck in the oxygen-rich water, raw sLFP and leaching residues obtained at various temperatures were characterised comprehensively. As shown in the X-ray diffraction (XRD) patterns (Fig. 2a), compared with raw sLFP, the LR-120, LR-150, and LR-180 samples retained the $LiFePO_4$ phase with an orthorhombic *Pnma* space group (JCPDS no. 40-1499). Therefore, in addition to the fact

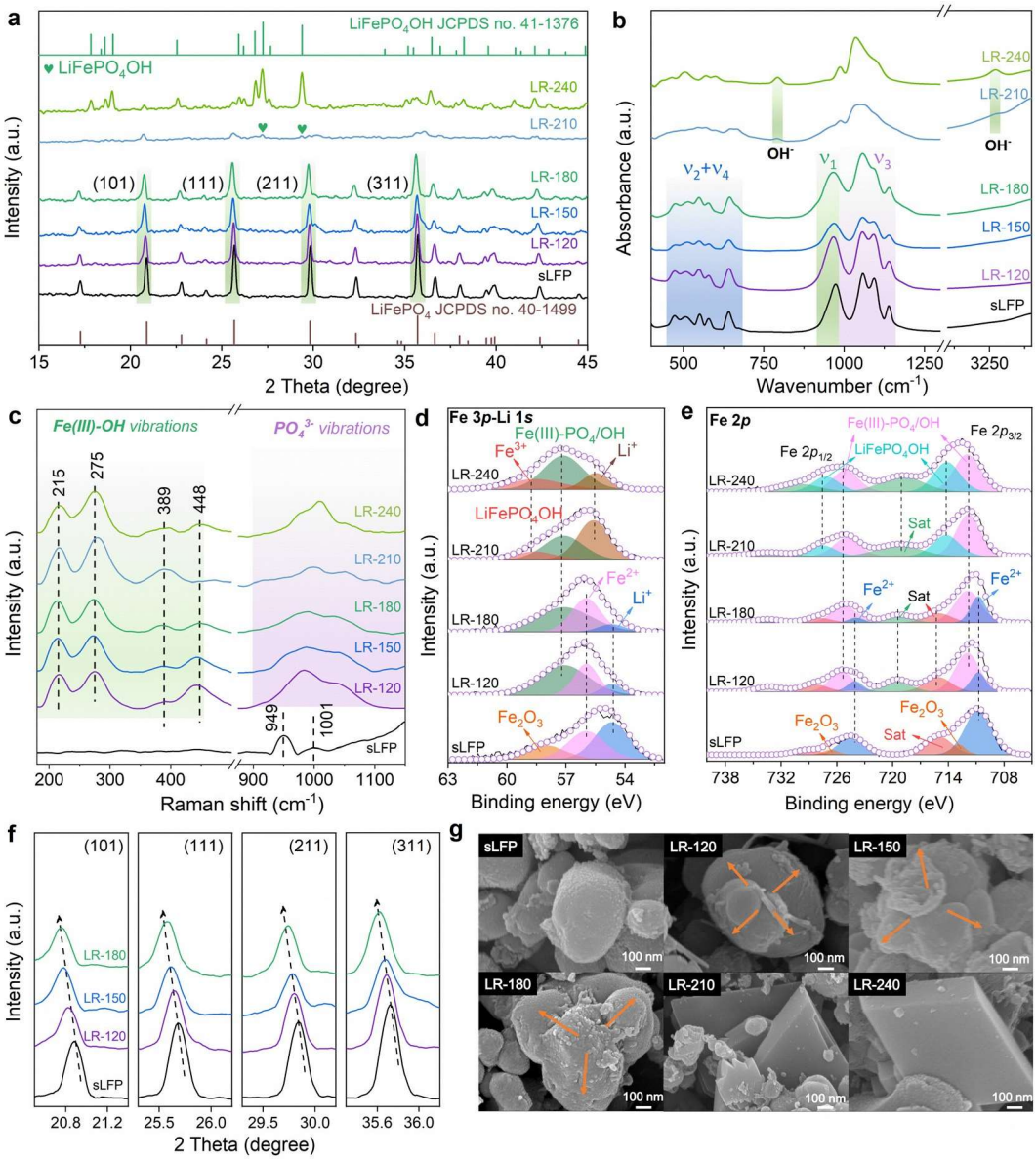

Fig. 2 (a) XRD patterns, (b) FTIR spectra, and (c) Raman spectra of raw sLFP and leaching residues obtained at various temperatures. (d) High-resolution XPS spectra of Fe 3p-Li 1s orbital, and (e) Fe 2p orbital. (f) Corresponding enlarged views of the (101), (111), (211), and (311) crystal planes and (g) SEM images of various samples.

that some Li and P elements were detected in the leachates (Fig. 1d), it was inferred that the redox reaction between sLFP and O_2 proceeded from the outer shell to the inner core of the sLFP particles. Specifically, the outer shell of the sLFP particles preferentially reacted and released Li and P species into the leachates, whereas the inner core of the sLFP particles retained its original olivine structure. As the temperature increased to 210 °C, the diffraction peaks indexed to LFP were almost absent, and a new phase emerged, which was indexed to tavorite hydroxyphosphate-$LiFePO_4OH$ (JCPDS no. 41-1376, denoted as LFPOH). The same phenomenon was observed in the LRs obtained at various partial oxygen pressures and leaching time (Fig. S2 and S3, ESI†), indicating that sLFP was almost completely oxidised by dissolved O_2 at 210 °C. As the temperature increased to 240 °C, the formed LFPOH phase is well-crystallized, which was accompanied by a decrease in the leaching efficiencies of Li and P. Fourier transform infrared spectroscopy (FTIR) of the LRs further confirmed this phenomenon. As shown in Fig. 2b, the typical bending (450–700 cm^{-1}, υ_2 and υ_4) and stretching vibrational (900–1150 cm^{-1}, υ_1 and υ_3) modes of PO_4^{3-} were present for the sLFP and LR samples.[29,30] The PO_4^{3-} vibration modes of the LR samples obtained below 180 °C were basically identical to that of sLFP, exhibiting the main phase is $LiFePO_4$. For the LR-210 sample, the peaks in the υ_2 and υ_4 regions disappeared, indicating that the coordination environment of PO_4^{3-} is disordered. However, these peaks reappeared as the temperature increased to 240 °C, indicating that PO_4^{3-} re-ordering occurs in the lattice. Notably, the emerging bands at 790 and 3273 cm^{-1} in LR-210 were further enhanced in LR-240, which confirms the formation of LFPOH.[31] Similar phenomenon was observed in the FTIR spectra of the LRs at various oxygen partial pressures and leaching times (Fig. S4, ESI†).

The undesired phase may be caused by gradual release of lithium and the reaction between Fe and OH^-/PO_4^{3-}. As shown in the Raman spectroscopy (Fig. 2c), the intense symmetric stretching peak observed at 944 cm^{-1} and the weak asymmetric stretching peak observed at 1001 cm^{-1} in the raw sLFP indicates the presence of non-distorted PO_4^{3-} species of LFP.[32] However, the local bonding environment of all the LRs exhibited similar features but changed significantly compared with that of the raw sLFP, as shown in Fig. 2c and Fig. S5 (ESI†). Some new peaks were observed at 215, 275, 389, and 488 cm^{-1}, which were identified as complex Fe(III)–OH species compared with the FeOOH and Fe_2O_3 reference samples (Table S2, ESI†). This may be attributed to $Fe(OH)_3$ dehydration at high temperatures. The broad peaks in the 900–1100 cm^{-1} region represent the vibrations of disordered PO_4^{3-}, indicating the presence of amorphous Fe(III)–PO_4 species. Thus, Fe^{3+} simultaneously reacts with OH^- and PO_4^{3-} as amorphous Fe(III)–PO_4/OH. The decomposition behaviour of sLFP toward oxidative and humid environment had been indicated in previous references on $LiFePO_4$ aging,[33–35] in which Li and phosphate species were dissolved and formed some undissolved Fe(III) phases (a-Fe_2O_3, $Li_xFePO_4OH_x$, and *et al.*). Considering an oxygen-rich aqueous environment were supplied for sLFP in this work, the sLFP decomposed to soluble $Li_xH_{3-x}PO_4$ and amorphous Fe(III)–PO_4/OH at a relative low temperature (≤180 °C). As the temperature reached up to 210 °C, partial $LiFePO_4OH$ crystalline phase was formed in the LRs, which trapped partial Li in the residues.

Further, the surface chemical states of the raw sLFP and LRs were characterized by X-ray photoelectron spectroscopy (XPS). As depicted in Fig. 2d, the peaks at 54.7 and 56.1 eV in the sLFP, LR-120, and LR-180 samples represent the characteristic peaks of Li^+ (Li 1s) and Fe^{2+} (Fe 3p) in $LiFePO_4$, respectively.[36,37] The areas of the two peaks decreased gradually as the temperature increased from 120 °C to 180 °C and finally disappeared at 210 °C, indicating that sLFP was effectively oxidised. Additionally, the Fe 3p peak centred at 57.4 eV after leaching may be attributed to the Fe(III)–PO_4/OH phase, because the binding energy is between the binding environment of Fe–PO_4 (57 eV)[38] and Fe–OH (57.6 eV).[39] For the LR-210 and LR-240 samples, the binding energy of Li^+ and Fe^{3+} increased to 55.6 and 58.9 eV, respectively, owing to the formed $LiFePO_4OH$ phase and strong electron-withdrawing characteristic of OH^-. Notably, the small peak observed at 58.2 eV of the Fe 3p orbital was attributed to Fe_2O_3,[40] which may be related to the oxidation of Fe^{2+} species during the cathode cycling process before retiring, as confirmed in the Fe 2p orbitals at 713.3 and 727.2 eV.[41] The binding energy of the Fe 2p orbital has a similar trend to that of Li 1s–Fe 3p, which increased with increasing temperature (Fig. 2e). The peaks located at 710.8 and 724.7 eV were attributed to the Fe^{2+} species in LFP.[42] However, these peaks disappeared above 210 °C, accompanied by the formation of Fe(III)–PO_4/OH (712.2 and 725.5 eV for $2p_{3/2}$ and $2p_{1/2}$) and LFPOH (714.4 and 727.7 eV for $2p_{3/2}$ and $2p_{1/2}$).

The amorphous iron phase can hinder the diffusion of reactants (O_2 and H_2O molecules) and products (Li^+ and PO_4^{3-}) in the leaching process, and the greater reaction degree of sLFP at higher temperature may be explained by the lattice swelling of the sLFP particles. As shown in Fig. 2f, the magnified (101), (111), (211), and (311) diffraction peaks of the sLFP, LR-120, LR-150, and LR-180 samples gradually shifted to a smaller angle as the temperature increased, indicating an expanded interplanar spacing based on the Bragg equation. As shown in Fig. 2g and Fig. S6–S11 (ESI†), the morphologies of sLFP and the LRs further confirmed lattice expansion. The particle size of the LR-120 sample was significantly larger than that of the raw sLFP. As the temperature increased to 180 °C, the spherical LFP particles gradually decomposed into deformed fine particles. Some well-crystallised rhombic particles were formed in the LRs at 210 and 240 °C, which is thought to be the LFPOH phase. The swelling of the LFP lattice can induce crack formation in the particles, which is beneficial for reactant diffusion and lithium leaching.

Transmission electron microscopy (TEM) images of LR-120 and LR-210 were compared to further elucidate the leaching mechanism. As shown in Fig. 3a, the shaded area spanning from the surface to the interior of the particle was amorphous (Fig. 3b) and may be composed of the formed Fe(III)–PO_4/OH phase. The remaining crystalline region was composed of unreacted LFP with an interplanar spacing of 2.56 Å (Fig. 3c), which is slightly larger than that of raw LFP material (2.52 Å),[43] demonstrating the lattice expansion of sLFP in the leaching

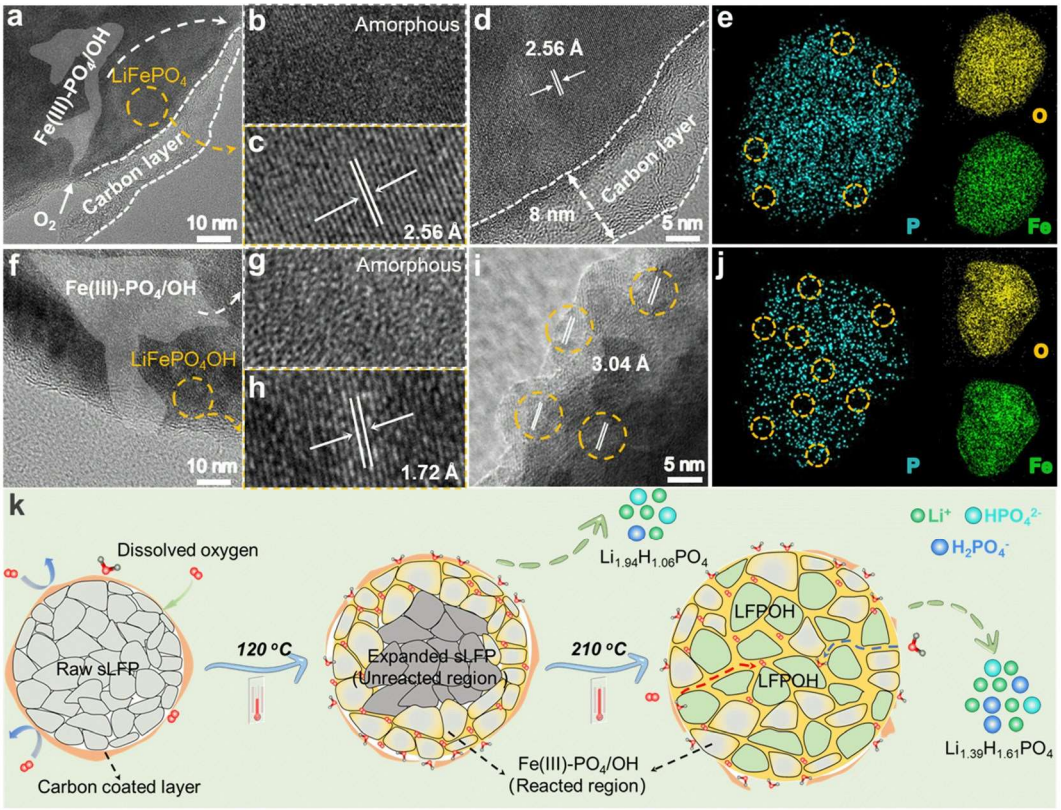

Fig. 3 Microstructure characterization of the LR-120 and LR-210 samples. (a-d) TEM images of LR-120; (f-i) TEM images of LR-210; EDS elemental mapping of P, O, and Fe for (e) LR-120 and (j) LR-210; (k) schematic of the leaching mechanism of sLFP in oxygen-rich water.

process. Additionally, a carbon coating layer with a thickness of approximately 8 nm was attached to the particle surface (Fig. 3a and d), which was further confirmed by FTIR spectra and elemental mapping (Fig. S12, ESI†). The presence of carbon layer can hinder the mass diffusion and the redox reaction, as directly demonstrated by the almost unreacted region under the carbon layer (Fig. 3d). The leaching reaction preferentially occurred on the sLFP particle surface with few carbon layer. Apart from the coated carbon, the effect of the PVDF binder and carbon additive on leaching was also explored with the untreated sLFP powders. Fig. S13 (ESI†) showed that the leaching efficiencies of the Li and P elements under various temperatures were close to the measured values in the treated sLFP samples (Fig. 1d), demonstrating the residual PVDF binder and carbon additives have minor effect on the element leaching.

As shown in Fig. 3f, the reacted region in the LR-210 sample was significantly larger than that in the LR-120 sample because of the thorough redox reaction. The measured interplanar spacing of 1.72 Å in Fig. 3h and 3.04 Å in Fig. 3i represent the (22-2) and (101) lattice planes of LFPOH, respectively,[31,44] indicating the crystallisation behaviour of the Li^{+}, Fe^{3+}, PO_4^{3-}, and OH^{-} species at the atomic level. As shown in Fig. 3e and j, energy dispersive X-ray spectroscopy (EDS) mapping images exhibited a homogeneous distribution of Fe and O in the two samples, whereas distinct ''vacancies'' were detected for P. This further confirms that partial P was leached with Li, whereas Fe and O were still trapped in the residue. In the LR-210 sample, P ''vacancies'' were observed in the inner particles, indicating that phosphate species migrated in the LFP crystal lattice during the water leaching process.

Fig. 3k shows the leaching mechanism of sLFP in the oxygen-rich water system. When the temperature is relatively low (120 ıC), the redox reaction mainly occurs in the outer shell of the sLFP particles, where more water molecules can participate in the primary hydrolysis of the released PO_4^{3-}. However, the mass transfer limitations caused by the *in situ* formed amorphous Fe(III)–PO_4/OH phase and the carbon coating layer was apparent because of the relatively weak expansion degree at low temperature, thus passivating the unreacted sLFP core. As the temperature increased to 210 ıC, the mass transfer was enhanced owing to the significant lattice expansion, and the redox reaction between sLFP and O_2 was almost complete. However, the limited water molecules in the inner particles resulted in the enrichment of Li^{+}, Fe^{3+}, PO_4^{3-}, and OH^{-} ions, which induced the formation of the $LiFePO_4OH$ phase and the leaching bottleneck. The crystallization of the $LiFePO_4OH$ could be enhanced by high temperature and prolonged leaching time, and thus 210 ıC of reaction temperature and 2 h of reaction time was the optimal leaching conditions. Additionally, PO_4^{3-} should be highly hydrolysed to $H_2PO_4^{-}$ in the inner particles to yield sufficient OH^{-} to react with Fe, and subsequently $H_2PO_4^{-}$ anions migrate into the leachates to maintain

the built-in anionic equilibrium. Essentially, the uncontrollable formation of Fe(III)–PO_4/OH cause the leaching bottleneck in the oxygen-rich water systems.

To eliminate the leaching bottleneck and release the trapped lithium, quantitative phosphoric acid was supplied to the oxygen-rich water system. The introduction of phosphate anions may circumvent internal diffusion by rebuilding a new anionic equilibrium. The introduced protons are expected to neutralise the generated OH^- in a timely manner, which may prevent the *in situ* formation of amorphous Fe(III)–PO_4/OH and construct a diffusion channel for Li^+. The leaching experiments were conducted under optimised conditions (210 °C, 0.3 MPa, 2 h) coupled with a low stoichiometric H_3PO_4 ratio (H_3PO_4/Li = 0.2, 0.33, or 1). The obtained leachates were named L-$HP_{0.2}$, L-$HP_{0.33}$, and L-HP_1, and the LRs were denoted as LR-$HP_{0.2}$, LR-$HP_{0.33}$, and LR-HP_1, respectively. Based on the measured element concentration in the Table S3 (ESI†), the leaching efficiencies of lithium for L-$HP_{0.2}$, L-$HP_{0.33}$, and L-HP_1 were calculated as 60.3%, 91.6%, and 95.1%, respectively (Fig. 4a), demonstrating the successful liberation of captured Li at a relatively low stoichiometric ratio of H_3PO_4 (0.33). Notably, the leached lithium may regenerate precipitates owing to the anionic equilibrium of the solution. Additionally, the P concentration in the leachates (Table S3, ESI†) was determined to calculate the Li/P molar ratio. As shown in Fig. 4b, the Li/P ratio in L-$HP_{0.2}$ and L-$HP_{0.33}$ were 1.72 and 1.62, respectively, indicating the coexistence of LiH_2PO_4 and Li_2HPO_4 in the leachates. In contrast, the Li/P ratio in L-HP_1 was only 0.76, which is lower than 1, indicating the coexistence of LiH_2PO_4 and unreacted H_3PO_4. The solution pH (Fig. 4b, right axis) of L-$HP_{0.33}$ and L-HP_1 was 2.45 and 2.18, respectively, indicating that many unreacted H^+ remained in the leachates.

The obtained LRs were characterised to elucidate the leaching mechanism in the H_3PO_4-supplied system. As shown in Fig. 4c, the XRD patterns of all the LRs exhibited that the LFPOH phase disappear and $Fe_5(PO_4)_4(OH)_3{\cdot}2H_2O$ (JCPDS no. 45-1436, denoted as FPOH) emerge. Small peaks were observed at 18.11, 20.71, 25.81, and 35.91, corresponding to $FePO_4$ (JCPDS no. 34-0134) in LR-HP_1, which may be generated by the reaction between FPOH and excess H_3PO_4. In addition, both the FTIR and Raman spectra of the three LRs (Fig. S14, ESI†) were similar and confirmed the formation of the FPOH phase.[45] The presence of the lithium-free FPOH phase further demonstrates that the leaching bottleneck of lithium in oxygen-rich water can be mitigated by quantitatively supplying H_3PO_4. For L-$HP_{0.2}$, partial Li may exist as Li_3PO_4 in the LRs based on the elemental distribution listed in Table S4 (ESI†). Thus, the low H_3PO_4 stoichiometry of 0.33 can effectively extract Li and prevent the formation of Li_3PO_4 deposition.

As shown in Fig. 4d, two fitting peaks were observed at 712.7 and 715.8 eV in the Fe $2p_{3/2}$ region for LR-$HP_{0.33}$ sample, corresponding to the bonding environments of Fe–PO_4 and

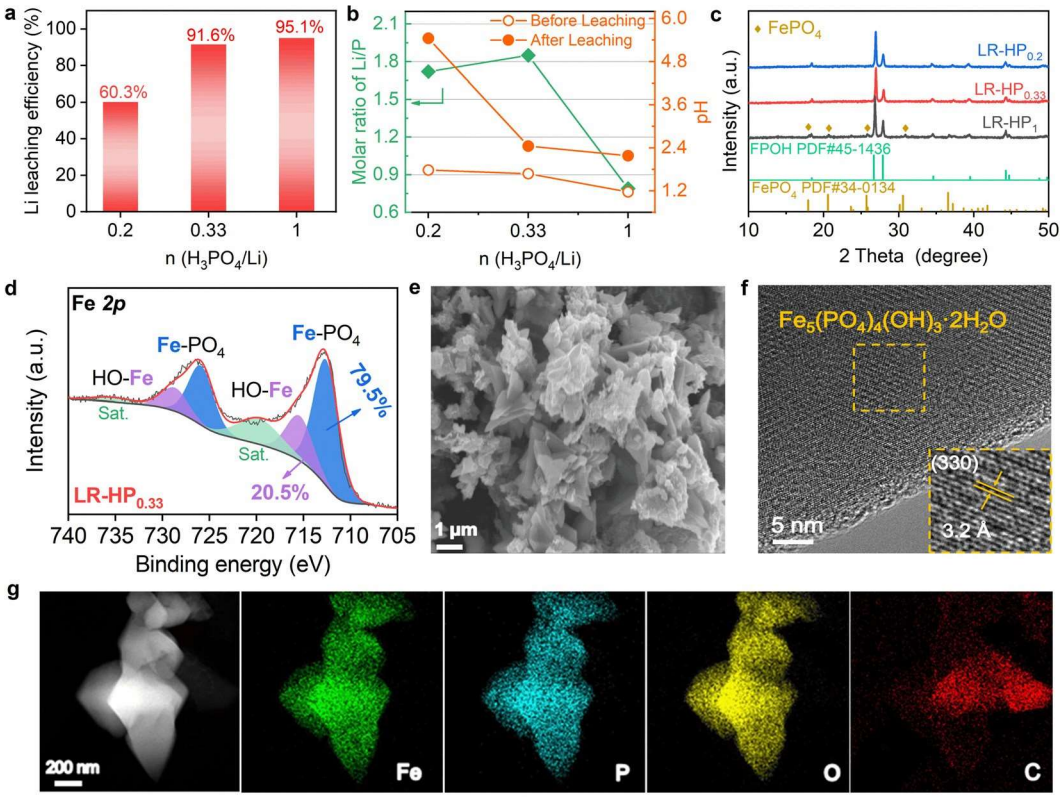

Fig. 4 Leaching behaviour of sLFP in the H_3PO_4-supplied system. (a) Leaching efficiency of Li; (b) elemental molar ratio of Li/P and solution pH; (c) XRD patterns of the leaching residues with various stoichiometric H_3PO_4 ratios; (d) high-resolution XPS spectrum of the Fe 2p orbital, (e) SEM image, (f) TEM image, and (g) EDS mapping of Fe, P, O, and C elements for the LR-$HP_{0.33}$ sample.

Fe–OH, respectively.[46] The area ratio of the two peaks was approximately 4 : 1, which corresponds to the composition of $Fe_5(PO_4)_4(OH)_3{\cdot}2H_2O$. A similar conclusion was drawn for the Fe 3p orbital (Fig. S15, ESI†). Additionally, the (330) crystal plane of the FPOH lattice (3.2 Å) in Fig. 4f and the uniformly distributed Fe, P, and O elements (Fig. 4g) further confirms the well-crystallised FPOH phase. As shown in Fig. 4e, the SEM image of the L-$HP_{0.33}$ sample exhibited the significant deformation of spherical sLFP particles to fusiform FPOH owing to the synergistic effect of H_3PO_4 and elevated temperature. Compared with the leaching behaviour of sLFP in oxygen-rich water, the supplied quantitative H_3PO_4 induced the formation of a well-crystallised FPOH phase, which serves as an excellent diffusion channel for both the reactants (H^+, H_2O, and O_2) and Li^+. Additionally, both released and supplied phosphate species balance the leached Li^+, thereby rebuilding the anionic equilibrium. Based on the measured P concentration and the amount of the supplied H_3PO_4, it could be calculated that 20.57% of PO_4^{3-} were leached from the sLFP in the L-$HP_{0.33}$ (detailed in the Table S5, ESI†), which was consistent with the missing amount of P element in the FPOH residue. Consequently, the degraded $LiFePO_4$ phase evolved into a fusiform $Fe_5(PO_4)_4(OH)_3{\cdot}2H_2O$ crystal, and 91.6% of Li and 20.57% of PO_4^{3-} were selectively extracted from sLFP as soluble $Li_{1.62}H_{1.38}PO_4$ at a H_3PO_4/$LiFePO_4$ molar ratio of 0.33. Regarding the obtained FPOH residues, several studies have been reported on their innovative synthesis and potential application in the fields of adsorption[47] and energy storage.[45,46]

To avoid introducing impurities, stoichiometric LiOH (1.5 M) was added to the concentrated L-$HP_{0.33}$ to recover the soluble $Li_{1.62}H_{1.38}PO_4$ as Li_3PO_4. As the solution pH increased to 5.5, white precipitates began to form. The precipitation reaction was finished as the pH increased to 8.0, and the consumed LiOH volume was 27 mL. Based on the element concentrations before and after precipitation (Table S6, ESI†), the Li and P recovery efficiency from the initial sLFP to the final Li_3PO_4 product (confirmed by XRD in Fig. 5b) was calculated as 90.19% and 19.88%, respectively. After recovering lithium, the mother liquor containing low concentration of elements (Table S6, ESI†) could be recycled for the subsequent leaching process, thus achieving sustainable waste-free recycling technology through the built-in anionic equilibrium mechanism, as illustrated in Fig. 5a. In the oxygen-rich water leaching system, limited PO_4^{3-} is released into the leachates for the equilibrium of Li^+, whereas residual PO_4^{3-} and the generated OH^- return to the residues. However, the undesired formation of the $LiFePO_4OH$ phase causes a bottleneck for Li leaching, which was always lower than two-thirds. After supplying stoichiometric H_3PO_4, sufficient H^+ converts Fe(III)–PO_4OH and $LiFePO_4OH$ into lithium-free $Fe_5(PO_4)_4(OH)_3{\cdot}2H_2O$. Both the introduced and released PO_4^{3-} species balances Li^+ to form soluble $Li_{1.85}H_{1.15}PO_4$ in the leachates, which is finally recovered as Li_3PO_4.

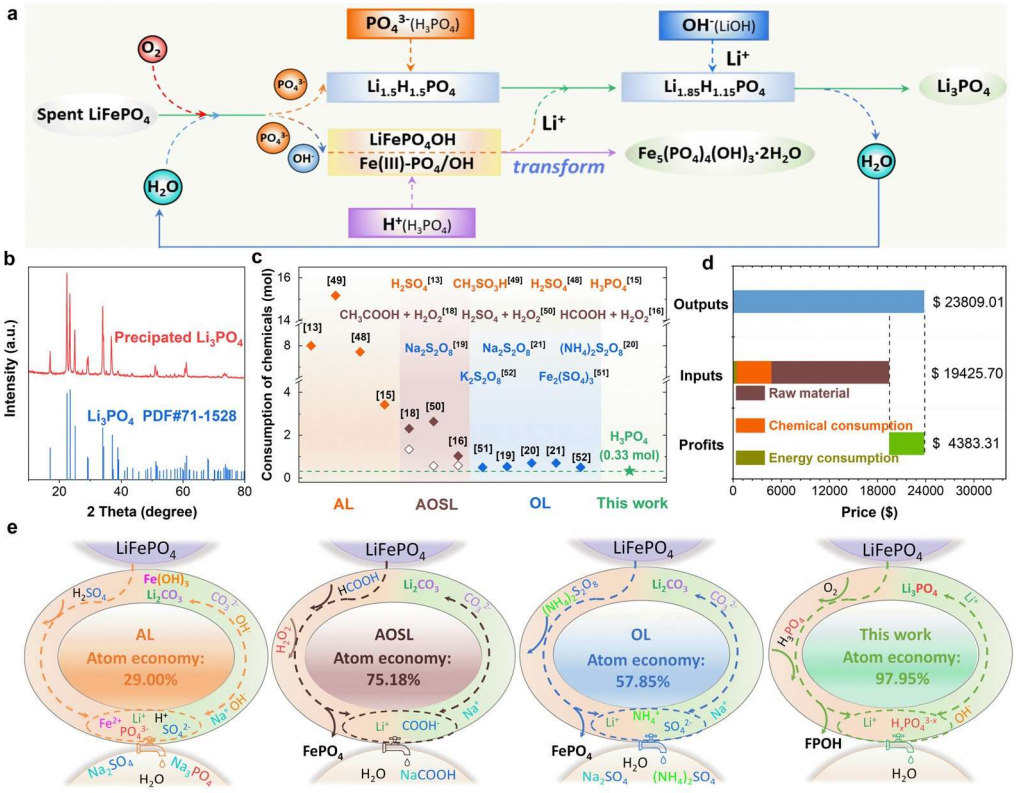

Fig. 5 (a) Illustration of the proposed built-in anionic equilibrium strategy for sLFP recycling; (b) XRD pattern of the obtained Li product; (c) comparison of reagent consumption and (e) atomic economy between reported AL, AOSL, OL processes and the strategy developed in this work; (d) economic assessment for recycling 1 ton of sLFP cathode with the proposed recovery strategy.

To evaluate the advantages of the proposed built-in anionic equilibrium recycling technology compared to the reported acid leaching (AL), acid/oxidant synergistic leaching (AOSL), and oxidation leaching (OL) technologies, chemical consumption and atom economy assessments were conducted. Considering that the reported literature mainly discusses the technological parameters, such as reagent concentration, solid/liquid ratio, and temperature, the specific stoichiometry usage was calculated based on the known data, as listed in Table S7 (ESI†). As shown in Fig. 5c, approximately 3.16–8 mol of strong inorganic acids were required to dissolve one mole of $LiFePO_4$ in AL technology.[13,15,48] When using weak organic acids as leachants, such as methyl sulfonic acid (CH_3SO_3H) and *p*-toluene sulfonic acid ($CH_3C_6H_4SO_3H$),[49] the acid consumption was increased to 15.17 mol owing to its stable olivine structure. Compared with the individual H_3PO_4 leaching process,[15] the introduction of O_2 in this work achieved the selective leaching of Li and provided built-in anion (OH^-) in the leaching process, which reduced the H_3PO_4 consumption from 3.16 mol to 0.33 mol for one mole $LiFePO_4$ (Fig. 5c). The recovery process was also simplified without an additional step to separate Li and Fe, as depicted in Fig. S16 (ESI†). AOSL technology enables the one-step separation of Fe and Li without structural degradation, which is more eco-friendly and improves acid utilisation. The total chemical consumption was 1.03–2.64 mol with the assistance of oxidants.[18,50] For the OL technology, selective Li extraction driven by individual strong oxidants further lowered the chemical consumption to 0.5–0.7 mol,[19–21,51,52] which is very similar to their theoretical stoichiometric usage. In this study, the lowest stoichiometric usage (0.33 mol) was achieved because of the built-in anionic equilibrium strategy, in which the added H_3PO_4 was utilised with high efficiency.

Combined with subsequent recovery steps, the atomic economy of the entire recycling process was calculated. Typical H_2SO_4, $HCOOH/H_2O_2$, and $(NH_4)_2S_2O_8$ leaching systems were selected as examples for the atom economy calculations for the AL, AOSL, and OL technologies, respectively, as shown in Fig. S17 (ESI†). As shown in Fig. 5e, the atomic efficiency for the AL process was calculated to be 29.00% owing to the wastage of the large amount of released PO_4^{3-} and the introduced SO_4^{2-} or Na^+ ions after Li recovery, which results in large quantities of saline wastewater containing Na_2SO_4 or Na_3PO_4, respectively. For the AOSL and OL processes, the atomic efficiencies were calculated to be 75.18% and 57.85%, respectively, which are higher than that of the AL process owing to the selective extraction of Li. However, the generation of secondary pollutants derived from NaCOOH or $(NH_4)_2SO_4$ is inevitable. Benefiting from the built-in anionic equilibrium mechanism, an atom economy of 97.95% can be achieved for lithium recycling from sLFP. All the involved elements originate from the reactants (sLFP, H_3PO_4, and LiOH) and end up in the products (Li_3PO_4 and $Fe_5(PO_4)_4(OH)_3{\cdot}2H_2O$), which reduces the ecological and environmental footprint of sLFP batteries.

Finally, an economic comparison analysis between the proposed recycling technology and conventional H_2O_2 recycling method[53] was conducted, as shown in Fig. 5d and Fig. S18 (ESI†). The primary inputs in the recycling process consisted mainly of raw materials and chemical and energy consumption. The outputs were calculated based on the obtained Li_3PO_4 products. The specific chemical costs were listed in Table S8 (ESI†) and the detailed evaluation processes were provided in the ESI.† The inputs and outputs for disposing of 1 ton of sLFP cathode materials were calculated to be \$19 425.70 and \$23 809.01, respectively. Thus, the profits were estimated to be 4383.31 \$ ton^{-1}, which is higher than the 1817 \$ ton^{-1} in the conventional H_2O_2 recycling method.[53] Both the reduced chemical consumption and co-extraction of ß20% PO_4^{3-} improve the recycling economy.

The industrial-scale application of the proposed recycling technology for sLFP could be foreseeable, considering that the pressure leaching has been widely used in the hydrometallurgy processes of non-ferrous metals resources.[54,55] Therefore, the scaled-up autoclave can be directly applied for recycling sLFP, especially under the condition of low acid concentration. The universality of the proposed built-in anionic equilibrium recycling strategy toward spent $LiCoO_2$ and $LiNi_xCo_yMn_zO_2$ ($x + y + z = 1$) was also explored preliminarily. Both the leaching efficiency of Li achieved 60% for spent $LiCoO_2$ and $LiNi_{1/3}Co_{1/3}Mn_{1/3}O_2$ under a reductive SO_2 atmosphere, demonstrating the proposed methodology was suitable for mainstream cathodes. The XRD patterns of the leaching residues in Fig. S19 (ESI†) also verified the phase change of $LiCoO_2$ and $LiNi_{1/3}Co_{1/3}Mn_{1/3}O_2$ during lithium leaching. Nonetheless, the authors realized that the involved chemical composition in this study focused on the Li–Fe–P–H_2O system. The proposed technology could be directly applied to recycle the electrode leftovers with uniform composition, while potential challenges might be existed in recycling the retired batteries. The black mass obtained from currently developed battery disassembly technology contains a large amount of Cu/Al current collectors (ο5 wt%), waste graphite, and other impurities, which might bring tedious separation and purification steps for the leaching residues after selective Li extraction. If the refined and automated battery disassembly can be performed, the feasibility and impact of the proposed recycling technology will largely be improved. Further study on the recovery of cathode black mass with complex composition will also help to enhance the industrial adoption for the proposed approach.

Conclusion

In this study, a built-in anionic equilibrium strategy was proposed for the sustainable recycling of sLFP. The feasibility of selective Li extraction in deionized water under oxygen pressure was confirmed. Both the oxygen reduction-induced hydroxyl and $LiFePO_4$-released phosphate promoted the selective extraction of lithium. Phase analysis of the residues revealed that the formation of a Li-trapped $LiFePO_4OH$ phase caused Li leaching bottleneck of 65.6%. Based on the built-in anionic equilibrium mechanism, a quantitative H_3PO_4-supplied strategy ($H_3PO_4/Li = 0.33$) was developed to enhance Li leaching from sLFP. The introduced H^+ and PO_4^{3-} induce phase reconstruction

and anion equilibrium with Li^+, respectively. The degraded $LiFePO_4$ phase evolved into a fusiform $Fe_5(PO_4)_4(OH)_3{\cdot}2H_2O$ crystal, and 90.19% of lithium and 19.88% of phosphorus in sLFP can be recovered as Li_3PO_4 product. Compared to existing sLFP disposal methods, the proposed built-in anionic equilibrium strategy exhibited lower chemical consumption, high economic value, and high atom economy, thus contributed to sustainable recycling of spent LFP batteries.

Experimental procedures

Materials and chemicals

Spent LFP pouch cells were supplied by Hunan Tiantai Tianrun Amperex Technology Co. Ltd, China. The sLFP powder was scraped and collected from the cathode and successively washed with *N*-methyl pyrrolidone and a dilute NaOH solution to remove the organic substrates and metal aluminium, respectively. The mass fractions of major elements (wt%) were 3.47% Li, 32.05% Fe, 17.72% P, and 0.04% Al. The elemental molar ratios of the Li/Fe and Fe/P were calculated as 0.871 and 1.003 (Table S9, ESI†), respectively, indicating the average composition of $Li_{0.87}FePO_4$ in the sLFP powder. Phosphoric acid (H_3PO_4; 85 wt%) and lithium hydroxide (LiOH) were purchased from Shanghai Macklin Biochemical Technology Co. Ltd. All chemical reagents were of analytical grade and were used without further purification. Deionised water was used throughout the experiments.

Selective leaching of sLFP

All the leaching experiments were conducted in an autoclave (1 L, Fig. 1a). A cooling coil was used to maintain a temperature fluctuation within 5 ıC during the leaching process and the rapid cooling of the lixiviums after leaching. The slurry consisted of sLFP powder and deionised water mixed at a solid–liquid ratio of 20 g L^{-1} (10 g sLFP powder and 500 mL of water). When the slurry was transferred to the autoclave, the impeller speed was set at 300 rpm. When the temperature reached the set value and the monitored pressure gauge was stabilised, oxygen gas with the desired partial pressure was introduced into the autoclave *via* the inlet valve. The gas sparger used was beneficial for the dispersion of oxygen and the contact between sLFP and O_2. The effects of the leaching temperature, oxygen partial pressure, and leaching time were evaluated for selective lithium extraction. A similar procedure was used for the stoichiometric H_3PO_4-supplied leaching experiments. 10 g of the sLFP powder was firstly mixed with 500 mL solution containing the desired amount of H_3PO_4 before being transferred to the autoclave. The adding H_3PO_4 concentration was 0.02, 0.033, and 0.1 mol L^{-1} to maintain the H_3PO_4/Li molar ratio of 0.2, 0.33, and 1.0, respectively. The specific H_3PO_4 adding amounts were detailed in Table S10 (ESI†).

After leaching, the autoclave was cooled to 25 ıC and the pressure was released *via* the outlet valve. The lixiviums were filtered to collect the leachates and LRs. The leaching efficiencies of the various elements in leachates were calculated as follows:

$$Z = \frac{c \times V}{m \times w\%}$$

where Z is the leaching efficiency and c, V, m, and w represent the ion concentration (mg L^{-1}), solution volume (L), material mass (mg), and mass percentage of each element, respectively.

All the residues were washed with deionised water twice and dried at 80 ıC overnight before characterisation. To quantify the chemical composition (Li, Fe, and P), the residues were completely dissolved in aqua regia (HNO_3 : HCl = 1 : 3, v/v) at 343 K for 5 h, and the digestion experiments were repeated three times to avoid sampling errors. The theoretical value of Fe/Li and Fe/P elemental molar ratio in residues could be calculated based on the initial elemental composition ($Li_{0.87}FePO_4$) and the leaching efficiency of Li/P in the leachates, as follow:

$$Fe/Li = \frac{100}{87.1 \times (1 - Z_{Li})}$$

$$Fe/P = \frac{1.003}{1 - Z_P}$$

Recovery of the Li product

Leachates containing Li^+ and protonated phosphate (HPO_4^{2-}/$H_2PO_4^-$) were recovered as Li_3PO_4 by the addition of LiOH. To improve the recovery efficiency of Li and P, the obtained leachates were first evaporated at 100 ıC to concentrate the Li to approximately 20 g L^{-1}. As the temperature dropped to 50 ıC, 1.5 M LiOH solution was slowly added into the concentrated leachates with magnetic stirring for 10 min. The solution pH was monitored during the precipitation process, and the LiOH amount was determined by the added solution volume. The obtained Li_3PO_4 precipitates was washed several times with deionised water and dried at 80 ıC in air.

Characterisation

The elemental concentrations in the leachates were analysed using inductively coupled plasma-atomic emission spectrometry (ICP-AES; Optima 3000DV, PerkinElmer Instrument). The pH of the solution was measured at 25 ıC using a pH meter (PHS-3C, Shanghai INESA Scientific Instrument Co., Ltd). The crystal structures of sLFP and the LRs were characterised by powder XRD (RIGAKU Ultima IV) with Cu Ka radiation. The structural information was characterised using a Fourier transform infrared spectrometer (Nicolet-6700, Thermo Scientific) in the region of 400–4000 cm^{-1} and a Raman spectrometer (Renishaw, inVia Reflex) with 532 nm incident laser light. The surface chemical states were characterized using XPS (Thermo Scientific K-Alpha) with Al Ka radiation. High-resolution field-emission scanning electron microscopy (FESEM; JEOL, JSM-7610FPlus, Japan) was used to monitor particle morphologies. The micromorphology and elemental mapping were determined using TEM (TEM, JEOL, JEM-F200, Japan) equipped with an EDS detector.

Author contributions

Pengfei Zhu: methodology, investigation, writing-original draft. Zhipeng Jiang: methodology, investigation. Wei Sun: validation. Yue Yang: resources. Debbie S. Silvester: validation. Hongshuai Hou: formal analysis. Craig E. Banks: methodology. Jiugang Hu: conceptualization, methodology, funding acquisition, writing-review & editing. Xiaobo Ji: methodology, supervision.

Conflicts of interest

There are no conflicts to declare.

Acknowledgements

This work was financially supported by the National Key Research and Development Program of China (No. 2019YFC1907801), National Natural Science Foundation of China (No. 52174286), and Natural Science Foundation of Hunan Province in China (2023JJ10068).

References

1 X. Ma, L. Azhari and Y. Wang, *Chem*, 2021, 7, 2843–2847.
2 G. Harper, R. Sommerville, E. Kendrick, L. Driscoll, P. Slater, R. Stolkin, A. Walton, P. Christensen, O. Heidrich, S. Lambert, A. Abbott, K. Ryder, L. Gaines and P. Anderson, *Nature*, 2019, 575, 75–86.
3 C. Bauer, S. Burkhardt, N. P. Dasgupta, L. A. W. Ellingsen, L. L. Gaines, H. Hao, R. Hischier, L. B. Hu, Y. H. Huang, J. Janek, C. D. Liang, H. Li, J. Li, Y. X. Li, Y. C. Lu, W. Luo, L. F. Nazar, E. A. Olivetti, J. F. Peters, J. L. M. Rupp, M. Weil, J. F. Whitacre and S. M. Xu, *Nat. Sustain.*, 2022, 5, 176–178.
4 R. E. Ciez and J. F. Whitacre, *Nat. Sustain.*, 2019, 2, 148–156.
5 Y. Yang, E. G. Okonkwo, G. Y. Huang, S. M. Xu, W. Sun and Y. H. He, *Energy Storage Mater.*, 2021, 36, 186–212.
6 E. Fan, L. Li, Z. Wang, J. Lin, Y. Huang, Y. Yao, R. Chen and F. Wu, *Chem. Rev.*, 2020, 120, 7020–7063.
7 P. P. Xu, Q. Dai, H. P. Gao, H. D. Liu, M. H. Zhang, M. Q. Li, Y. Chen, K. An, Y. S. Meng, P. Liu, Y. R. Li, J. S. Spangenberger, L. Gaines, J. Lu and Z. Chen, *Joule*, 2020, 4, 2609–2626.
8 M. Fan, Q. Meng, X. Chang, C. F. Gu, X. H. Meng, Y. X. Yin, H. Li, L. J. Wan and Y. G. Guo, *Adv. Energy Mater.*, 2022, 12, 2103630.
9 J. Ma, J. Wang, K. Jia, Z. Liang, G. Ji, Z. Zhuang, G. Zhou and H. M. Cheng, *J. Am. Chem. Soc.*, 2022, 144, 20306–20314.
10 X. Chang, M. Fan, C. F. Gu, W. H. He, Q. Meng, L. J. Wan and Y. G. Guo, *Angew. Chem., Int. Ed.*, 2022, 61, e202202558.
11 J. H. Tan, Q. Wang, S. Chen, Z. H. Li, J. Sun, W. Liu, W. S. Yang, X. Xiang, X. M. Sun and X. Duan, *Energy Storage Mater.*, 2021, 41, 380–394.
12 J. Kumar, R. R. Neiber, J. Park, R. A. Soomro, G. W. Greene, S. A. Mazari, H. Y. Seo, J. H. Lee, M. Shon, D. W. Chang and K. Y. Cho, *Chem. Eng. J.*, 2022, 431, 133993.
13 G. Q. Cai, K. Y. Fung, K. M. Ng and C. Wibowo, *Ind. Eng. Chem. Res.*, 2014, 53, 18245–18259.
14 J. Kumar, X. Shen, B. Li, H. Liu and J. Zhao, *Waste Manage.*, 2020, 113, 32–40.
15 D. C. Bian, Y. H. Sun, S. Li, Y. Tian, Z. H. Yang, X. M. Fan and W. X. Zhang, *Electrochim. Acta*, 2016, 190, 134–140.
16 H. Mahandra and A. Ghahreman, *Resour., Conserv. Recycl.*, 2021, 175, 105883.
17 Z. Jiang, P. Zhu, Y. Yang, W. Jin, G. Zou, H. Hou, J. Hu, W. Sun and X. Ji, *Chem. Eng. J.*, 2023, 466, 143186.
18 Y. X. Yang, X. Q. Meng, H. B. Cao, X. Lin, C. M. Liu, Y. Sun, Y. Zhang and Z. Sun, *Green Chem.*, 2018, 20, 3121–3133.
19 X. H. Yue, C. C. Zhang, W. B. Zhang, Y. F. Wang and F. S. Zhang, *Chem. Eng. J.*, 2021, 426, 131311.
20 D. Z. Peng, J. F. Zhang, J. T. Zou, G. J. Ji, L. Ye, D. M. Li, B. Zhang and X. Ou, *J. Cleaner Prod.*, 2021, 316, 128098.
21 J. L. Zhang, J. T. Hu, Y. B. Liu, Q. K. Jing, C. Yang, Y. Q. Chen and C. Y. Wang, *ACS Sustainable Chem. Eng.*, 2019, 7, 5626–5631.
22 X. J. Qiu, B. C. Zhang, Y. L. Xu, J. G. Hu, W. T. Deng, G. Q. Zou, H. S. Hou, Y. Yang, W. Sun, Y. H. Hu, X. Y. Cao and X. B. Ji, *Green Chem.*, 2022, 24, 2506–2515.
23 H. S. Xu, C. Wei, C. X. Li, G. Fan, Z. G. Deng, X. J. Zhou and S. Qiu, *Sep. Purif. Technol.*, 2012, 85, 206–212.
24 L. Wang, Y. Liu, Y. Lin, Y. Yu, X. Zhang, R. Zhang and Y. Zhai, *J. Alloys Compd.*, 2021, 887, 161424.
25 W. Peng, L. Jiao, H. Gao, Z. Qi, Q. Wang, H. Du, Y. Si, Y. Wang and H. Yuan, *J. Power Sources*, 2011, 196,2841–2847.
26 Y. Huan, S. X. Chen, R. Zeng, T. Wei, D. H. Dong, X. Hu and Y. H. Huang, *Adv. Energy Mater.*, 2019, 9, 1901573.
27 E. Nurlaela, T. Shinagawa, M. Qureshi, D. S. Dhawale and K. Takanabe, *ACS Catal.*, 2016, 6, 1713–1722.
28 J. Hu, W. Huang, L. Yang and F. Pan, *Nanoscale*, 2020, 12, 15036–15044.
29 Z. Ma, Z. Zuo, L. Li and Y. Li, *Adv. Funct. Mater.*, 2021, 32, 2108692.
30 C. M. Burba and R. Frech, *J. Electrochem. Soc.*, 2004, 151, A1032–A1038.
31 N. Marx, L. Croguennec, D. Carlier, L. Bourgeois, P. Kubiak, F. Le Cras and C. Delmas, *Chem. Mater.*, 2010, 22,1854–1861.
32 T. Yamanaka, T. Minato, K. Okazaki, T. Abe, K. Nishio and Z. Ogumi, *ACS Appl. Energy Mater.*, 2018, 1, 1140–1145.
33 J.-F. Martin, M. Cuisinier, N. Dupré, A. Yamada, R. Kanno and D. Guyomard, *J. Power Sources*, 2011, 196, 2155–2163.
34 K. Zaghib, M. Dontigny, P. Charest, J. F. Labrecque, A. Guerfi, M. Kopec, A. Mauger, F. Gendron and C. M. Julien, *J. Power Sources*, 2008, 185, 698–710.
35 X. Xia, Z. Wang and L. Chen, *Electrochem. Commun.*, 2008, 10, 1442–1444.
36 J. P. Baboo, M. A. Yatoo, M. Dent, E. H. Najafabadi, C. Lekakou, R. Slade, S. J. Hinder and J. F. Watts, *Energies*, 2022, 15, 2332.
37 W. Xiong, Q. Hub and S. Liu, *Anal. Methods*, 2014, 6,5708–5711.

38 R. Dedryvère, M. Maccario, L. Croguennec, F. Le Cras, C. Delmas and D. Gonbeau, *Chem. Mater.*, 2008, 20, 7164–7170.

39 K. Wang, A. F. Martinez, L. Simonelli, B. Made, P. Henocq, B. Ma and L. Charlet, *Environ. Sci. Technol.*, 2022, 56,5602–5610.

40 C. M. Tian, W. W. Li, Y. M. Lin, Z. Z. Yang, L. Wang, Y. G. Du, H. Y. Xiao, L. Qiao, J. Y. Zhang, L. Chen, D. C. Qi, J. L. MacManus-Driscoll and K. H. L. Zhang, *J. Phys. Chem. C*, 2020, 124, 12548–12558.

41 Y. X. Qin, Z. Z. Yang, J. J. Wang, Z. Y. Xie, M. Y. Cui, C. M. Tian, Y. G. Du and K. H. L. Zhang, *Appl. Surf. Sci.*, 2019, 464, 488–493.

42 H. Jin, J. L. Zhang, D. D. Wang, Q. K. Jing, Y. Q. Chen and C. Y. Wang, *Green Chem.*, 2022, 24, 152–162.

43 J. Lin, Y.-H. Sun and X. Lin, *Nano Energy*, 2022, 91, 106655.

44 L. Sharma, K. Nakamoto, S. Okada and P. Barpanda, *J. Power Sources*, 2019, 429, 17–21.

45 S. Han, J. Wang, S. Li, D. Wu and X. Feng, *J. Mater. Chem. A*, 2014, 2, 6174–6179.

46 V. Mani, G. N. Suresh babu and N. Kalaiselvi, *J. Power Sources*, 2018, 395, 31–40.

47 Q. Chen, C. Wei, Y. Zhang, H. Pang, Q. Lu and F. Gao, *Sci. Rep.*, 2014, 4, 3753.

48 Y. F. Song, B. Y. Xie, S. L. Song, S. Y. Lei, W. Sun, R. Xu and Y. Yang, *Green Chem.*, 2021, 23, 3963–3971.

49 P. Yadav, C. J. Jie, S. Tan and M. Srinivasan, *J. Hazard. Mater.*, 2020, 399, 123068.

50 H. Li, S. Z. Xing, Y. Liu, F. J. Li, H. Guo and G. Kuang, *ACS Sustainable Chem. Eng.*, 2017, 5, 8017–8024.

51 Y. Dai, Z. Xu, D. Hua, H. Gu and N. Wang, *J. Hazard. Mater.*, 2020, 396, 122707.

52 B. Gangaja, S. Nair and D. Santhanagopalan, *ACS Sustainable Chem. Eng.*, 2021, 9, 4711–4721.

53 H. Zhou, Z. Luo, S. Wang, X. Ma and Z. Cao, *Sep. Purif. Technol.*, 2023, 315, 123742.

54 J. Xi, G. Ji, Y. Liao, Y. Wu, Q. Liu and M. Li, *J. Sust. Metall.*, 2022, 8, 51–63.

55 S. Rao, Y. Liu, D. Wang, H. Cao, W. Zhu, R. Yang, L. Duan and Z. Liu, *J. Cleaner Prod.*, 2021, 278, 123989.